NAL-Conf-74/56-EXP

Rockefeller University
COO-2232A-1

University of Rochester
COO-3065-87 (UR 494)

PROTON-DEUTERON ELASTIC SCATTERING AND DIFFRACTION DISSOCIATION from 50 to 400 GeV*

Y. Akimov, L. Golovanov, S. Mukhin, G. Takhtamyshev, and V. Tsarev
Joint Institute for Nuclear Research, Dubna, U.S.S.R.

E. Malamud, R. Yamada, and P. Zimmerman
Fermi National Accelerator Laboratory, Batavia, Illinois

R. Cool, K. Goulianos, and H. Sticker
Rockefeller University, New York, New York

D. Gross, A. Melissinos, D. Nitz, and S. Olsen
University of Rochester, Rochester, New York

Submitted to the International Conference on High Energy Physics
London, 1 - 10 July 1974

---

* This work was performed under the auspices of the U. S. Atomic Energy Commission.

I. INTRODUCTION

In an experiment presently being conducted at the Fermi National Accelerator Laboratory (FERMILAB), we are studying the coherent, low four-momentum transfer interaction of high energy protons with a deuterium gas jet target,

$$p + d \rightarrow X + d \tag{1}$$

Both processes, elastic scattering and diffraction dissociation of the incoming beam proton, are being investigated by detection of the recoil deuteron. In this report, we present results on part of our data for incident proton energies from 50 to 400 GeV in the four-momentum transfer squared range $0.03 < |t| \lesssim 0.12$ $(GeV/c)^2$ and for $m_X^2 \lesssim 35$ $(GeV/c^2)^2$.

The interest in p-d elastic scattering is in probing the proton-neutron interaction. In addition, the elastic scattering data are used to extract the deuteron form factor squared, $F_d(t)$, which is essential in the analysis of the t distribution of the inelastic interactions.

In the process of diffraction dissociation, protons are excited coherently (no internal quantum number exchange) into high mass states. One is interested here in the invariant differential cross section

$$s \frac{d^2\sigma}{dm_X^2 dt} = f(s, m_X^2, t) \tag{2}$$

over as wide a range in the variables s and m_X^2 as possible. The excitation of a proton of mass m_p into a state of mass m_X requires a minimum four-momentum transfer to the deuteron of

$$|t|_{min}^{1/2} = \frac{m_x^2 - m_p^2}{s} m_d \tag{3}$$

For coherent excitation, the condition is[1]

$$|t|_{min}^{1/2} \lesssim m_\pi \tag{4}$$

where m_π is the mass of the pion. Thus, as s increases, the proton can be excited coherently into states of higher and higher mass. In terms of the Feynman scaling variable x, defined as $p_{\parallel} / p_{max}$ of the deuteron in the c.m. system, the square of the "missing" mass is given in our case by

$$m_x^2 \simeq m_p^2 + s(1-x) \tag{5}$$

and the coherence condition (4) can be written as

$$(1-x)\, m_d \lesssim m_\pi \tag{6}$$

With deuterons as target particles, s is given by

$$s \simeq 2m_d\, p_o \tag{7}$$

where p_o is the momentum of the incident proton. From (5), (6), and (7) one sees that mass-squared values as high as $m_x^2 \simeq m_p^2 + 2m_\pi p_o$, or $\sim 110\ (GeV/c^2)^2$ for $p_o = 400$ GeV/c, are allowed by the coherence condition.

There is, of course, interest in the inclusive process (1) for even higher values of m_x^2, even if coherence were to break down. We are presently analyzing data where m_x^2 reaches $\sim 150\ (\mathrm{GeV}/c^2)^2$, but in this report we present results only for $m_x^2 \lesssim 35\ (\mathrm{GeV}/c^2)^2$. The results we present here ($x \gtrsim 0.97$) are well within the coherence region.

To facilitate comparison of our inelastic data on $p + d \to X + d$ with existing data on $p + p \to X + p$ we divide our cross sections at a given t-value by the deuteron form factor squared $F_d(t)$. For this purpose, we use the function

$$F_d(t) = \left(\frac{\sigma_T^{pd}}{\sigma_T^{pp}} \right)^2 e^{b_F t + c_F t^2} \tag{8}$$

with[2] $b_F = 25.9\ (\pm 1.2)\ (\mathrm{GeV}/c)^{-2}$ and $c_F = 60\ (\pm 5)\ (\mathrm{GeV}/c)^{-4}$. Our elastic scattering data agree with these values but, at this point in time, the t-range of the analyzed data is small and our fits are not very sensitive to the value of c_F.

II. THE EXPERIMENT

The experiment is carried out using a deuterium gas jet target[3] inside the main ring of the NAL accelerator. The jet is pulsed to intercept the beam at predetermined times during the acceleration cycle, thus selecting the desired beam energies. Deuterons recoiling at large angles to the beam direction, $45^0 < \theta_d < 90^0$, are detected by an array of solid state detectors.

The recoil kinematics are particularly suited for the study of low t interactions of the incident protons. The four-momentum transfer is obtained

directly from a measurement of the kinetic energy T of the recoil deuteron,

$$|t| = 2m_d T \quad . \tag{9}$$

The mass of the "missing" particle X --reaction (1)--can be computed from $|t|$ and the angle θ of the deuteron with respect to the direction of the beam

$$m_x^2 \simeq m_p^2 + 2p_o \sqrt{|t|} \left[\cos\theta - \left(\frac{p_o + m_d}{p_o} \right) \frac{\sqrt{|t|}}{2m_d} \right] \tag{10}$$

For elastic scattering, $m_x^2 = m_p^2$, we have

$$\cos\theta_{el} \simeq \left(\frac{p_o + m_d}{p_o} \right) \frac{\sqrt{|t|}}{2m_d} \tag{11}$$

It is important to note that for $p_o >> m_d$, which is the case in this experiment, eq. (11) is nearly independent of the beam momentum. Thus, a single arrangement of detectors can be used to obtain elastic scattering data at any given beam momentum during the acceleration cycle of the machine. This is very useful, since our main interest is in the study of the variation of the elastic scattering parameters with energy. For inelastic scattering, combining of eqs. (5) and (10) yields

$$x \simeq 1 - \frac{\sqrt{|t|}}{m_d} \left[\cos\theta - \left(\frac{p_o + m_d}{p_o} \right) \frac{\sqrt{|t|}}{2m_d} \right] \tag{12}$$

which is also approximately independent of the beam momentum.

A schematic drawing of the apparatus is shown in Figure 1. The detectors are mounted on a carriage which can be moved to different angles with respect to the beam direction. Data are taken with the carriage at various angular positions and are normalized by the elastically scattered counts in one detector which is always kept in a fixed position. Each detector consists of a stack of two solid state counters. The first counter is typically 0.2mm thick and the second 1.5mm to 5mm thick. From pulse height measurements we determine the energies in MeV, T_1 and T_2, deposited by a particle in each counter of a stack. The mass of a particle stopping in the second counter is given by the empirical formula

$$m = m_p \left\{\frac{\alpha}{d_1}\left[(T_1+T_2)^{\beta} - T_2^{\beta}\right]\right\}^{1/(\beta-1)} \qquad (13)$$

where $\alpha = 0.0133$, $\beta = 1.73$, and d_1 is the thickness of the first counter in mm. A typical mass plot for particles registered by a stack during an actual run with a deuterium jet target is shown in Figure 2. The deuterons can be easily separated out. The protons come from break-up of the target deuteron and from general room background. The low mass events are mainly due to particles that penetrate both counters of the stack. The solid state counters are calibrated with an α source of 5.8 MeV.

III. DATA ANALYSIS

The recoil deuteron events are separated out and histogramed against their total energy, $T = T_1+T_2$. Figure 3 shows three such histograms for three different incident proton momenta. The large peak in each histogram

is due to elastically scattered deuterons that stop in the stack. The counts at recoil energies smaller than that of the elastic peak are mainly due to inelastic scattering. In the 50 GeV/c data, the elastic peaks are largely free of inelastics and the small background of $\lesssim 1\%$ (Fig. 3a) is due to recoils from residual deuterium gas in the beam pipe. To extract the elastic counts, this background is removed by interpolation under the peak. As the beam momentum increases, the inelastics move closer to the elastic peak as expected from eq. (10) and seen in Figures 3b and 3c. The extraction of the elastic counts at these higher beam energies is accomplished with the help of the knowledge of the shape of the elastic peaks obtained from the 50 GeV/c data. The inelastic counts ΔN in a given interval Δt are then reduced to differential cross sections using the formula

$$\frac{d^2\sigma}{dm_x^2 dt} = \left[\frac{(d\sigma/d\Omega)_{el}}{N_{el}}\right]_{\text{fixed detector}} \frac{\Delta N}{\Delta t} \frac{\pi}{p_o\sqrt{|t|}}$$

where N_{el} is the number of elastic deuteron recoils registered by the fixed detector (monitor) during the run, and $(d\sigma/d\Omega)_{el}$ is the elastic scattering differential cross section at the angular position of the fixed detector. This cross section is calculated with the formula

$$\left(\frac{d\sigma}{d\Omega}\right)_{el} = \frac{p_o}{p_o+md} \frac{2md\sqrt{|t|}}{\pi} \left[(\sigma_T^{pd})^2 \frac{1+\rho_{pd}^2}{16\pi}\right] e^{bt+ct^2} \qquad (15)$$

where the term in the brackets is the optical point, $(\frac{d\sigma}{dt})_{el}$ $(t = 0)$. We have used the values of b measured in this experiment, and fixed $c = 60\ (GeV/c)^{-4}$ obtained from Ref. (8), and used the total p-d cross sections measured in a recent experiment[4] at FERMILAB in the range $50 < p_o < 200$ GeV/c. For $p_o > 200$ GeV/c, we have assumed that the total p-d cross section rises with energy by the same proportion as the total p-p cross section[5]. For ρ_{pd}, the ratio of the real to the imaginary part of the forward scattering amplitude, we used the value[6] $\rho = 0.17$ at $p_o = 50$ GeV/c and we set $\rho = 0$ at our higher beam energies.

IV. ELASTIC SCATTERING

The elastic scattering differential cross sections extracted from our data in the interval $0.05 \lesssim |t| \lesssim 0.12\ (GeV/c)^2$ were fitted by the function

$$\frac{d\sigma}{dt}(s,t) = \frac{d\sigma}{dt}(s,t = 0)\ e^{b(s)t+ct^2} \qquad (16)$$

Due to the small t-range of our present data, the fits are not very sensitive to the parameter c. On the other hand, the values of $b(s)$ obtained are correlated to c. Since c is not expected to have a strong energy dependence within our t-range, we fitted our data keeping c fixed at the value of[2] $60\ (GeV/c)^{-4}$ and we obtained $b(s)$ at eight different s-values. Figure 4 shows the elastic differential cross section as a function of t for two different beam momenta, 50 GeV/c and 385 GeV/c. The curves have been normalized to the same value at $t = 0$ in order to display the

shrinkage of the elastic peak with increasing energy. In Figure 5 we plot the parameters b(s) as a function of $\ln s$. The solid line is a fit to the form

$$b(s) = b_o^{pd} + 2\,\alpha'_{pd}\,\ln s \tag{17}$$

We find $b_o^{pd} = 35.7 \pm 1.1\ (\mathrm{GeV/c})^{-2}$ and $2\alpha'_{pd} = 0.73 \pm 0.17\ (\mathrm{GeV/c})^{-2}$ as compared to the values for p-p scattering[3] of $b_o^{pp} = 8.23 \pm 0.27$ and $2\alpha'_{pp} = 0.55 \pm 0.048\ (\mathrm{GeV/c})^{-2}$.

Within the experimental errors, the shrinkage of the diffraction peak in p-d elastic scattering is the same as that in p-p scattering. The Glauber corrections have a very small effect on α', $\lesssim 2\%$. We therefore conclude that, within errors, the parameter α'_{pn} for p-n scattering is the same as α'_{pp} for p-p scattering. Assuming that $b_o^{pp} = b_o^{pn}$, we calculate that $b_o^{pd} = b_o^{pp} + b_F$(of eq. 8) + $\sim$1.5 (Glauber correction) $\simeq 35.6\ (\mathrm{GeV/c})^{-2}$, in good agreement with our value of 35.7 ± 1.1. Thus, our results are consistent with the form factor of eq. (8) as determined at lower energies[2].

V. DIFFRACTION DISSOCIATION

Our data on inelastic proton-deuteron scattering are in the range $0.03 \leq |t| \lesssim 0.12$ $(GeV/c)^2$, $190 < s < 1450$ GeV^2, and $(1-m_p^2/s) \lesssim x \lesssim 0.97$. Our results, divided by the deuteron form factor given by eq. (8), are presented in Figures 6 through 12. The "missing" mass resolution is limited by the uncertainty in the measurement of the angle θ of the recoil deuteron, $\Delta\theta = \pm 2.7$ mrad, and is given by

$$m_x^2 = 2p_o \sqrt{|t|}\, \Delta\theta \tag{18}$$

which has values between $\Delta m_x^2(p_o = 50, |t| = 0.03) = \pm 0.05$ and $\Delta m_x^2(p_o = 400, |t| = 0.12) = \pm 0.75$ $(GeV/c^2)^2$. The incident proton momentum is measured to ± 1.5 GeV/c using the accelerator magnet ramp, but the spread in momentum for the data we present here is about ± 5 GeV/c contributing to the mass width an amount $\Delta m_x^2/m_x^2 = \Delta p_o/p_o$ which is about $\pm 10\%$ in the worst case of $p_o = 50$ GeV/c.

Our results show the following features:

1. Energy Dependence -

Our cross sections are consistent with energy independence to within $\sim 10\%$ over our entire missing mass range within $x \gtrsim 0.97$. However, the 50 GeV/c data do seem consistently higher. We are presently investigating the possibility of an energy dependence $\lesssim 10\%$.

2. Low Mass Spectrum and Factorization -

The low mass spectrum, $m_x^2 \lesssim 6$ $(GeV/c^2)^2$, is dominated by a large peak at $m_x^2 \simeq 1.8$ $(GeV/c^2)^2$. In Figure 6, we compare our results for

$p + d \to x + d$ at a fixed t interval, $0.03 < |t| < 0.04$ $(GeV/c)^2$, with similar results[7] for $p + p \to x + p$. Within the experimental uncertainties of $\sim 20\%$, the two results are the same, consistent with factorization of the inelastic vertex in these two reactions.

3. High Mass Spectrum -

In Figure 7, we present cross section values multiplied by m_x^2 as a function of m_x^2 in the interval $0.03 < |t| < 0.04$ $(GeV/c)^2$ for various beam energies. We observe that, for $m_x^2 \gtrsim 6$ $(GeV/c^2)^2$, within our errors the points lie on a horizontal line, indicating a $1/m_x^2$ behavior for the cross sections. The same behavior is observed for other t values in this mass region. These results are consistent with triple pomeron[8] dominance in the diffraction dissociation process.

4. Slope Parameter -

The data at fixed m_x^2 were fitted by the function

$$\left[\frac{d^2\sigma}{dm_x^2 dt}\right]_{m_x^2} = \left[\frac{d^2\sigma}{dm_x^2 dt}\right]_{m_x^2, t=0} e^{-b(m_x^2)\,|t|} \qquad (19)$$

in the interval $0.03 < |t| \lesssim 0.12$ $(GeV/c)^2$. The fits were generally good and yielded positive values for the slope parameter $b(m_x^2)$. A typical differential cross section $d\sigma/dt$ is shown in Figure 8. Our results for $b(m_x^2)$ as a function of m_x^2 are presented in Figure 9. The slope parameters appear to be energy independent. As a function of m_x^2, they decrease rapidly from the value of ~ 18 $(GeV/c)^{-2}$ at $m_x^2 \sim 1.8$ $(GeV/c^2)^2$

to become constant, within errors, at the approximate value of $\sim 5.5\ (\mathrm{GeV/c})^{-2}$ for $m_X^2 \gtrsim 6\ (\mathrm{GeV/c^2})^2$.

5. Integral over t -

In addition to yielding the slopes, the fits of the data by eq. (19) also yielded the differential cross section values at $t = 0$. These are presented in Figure 10 multiplied by m_X^2. Comparing with Figure 7, we notice that while the $1/m_X^2$ dependence still holds for the high mass region, the low mass peak is sharper at $t = 0$. Comparison with Figure 9 shows that the slopes $b(m_X^2)$ are proportional to the values of the cross sections at $t = 0$ multiplied by m_X^2. Thus, the integral of the differential cross section over t multiplied by m_X^2 seems to be a constant independent of s and m_X^2 for all mass values in our interval of $x \gtrsim 0.97$. This is displayed in Figure 11. The diffraction dissociation cross section may then be written as

$$\frac{d^2\sigma}{dm_X^2 dt} = \frac{A(m_X^2,s)}{m_X^2}\, b(m_X^2)\, e^{-b(m_X^2)\cdot|t|} \tag{20}$$

and the integral of this cross section over t as

$$\frac{d\sigma}{dm_X^2} = \frac{A(m_X^2,s)}{m_X^2} \tag{21}$$

where $A(m_X^2,s)$ is approximately constant and equal to ~ 0.7 mb. In terms of the Feynman scaling variable x, eq. (21) takes the form

$$\frac{d\sigma}{dx} = \frac{A}{1 - x + \frac{m_p^2}{s}} \qquad (22)$$

which suggest the plot of $\ell n(d\sigma/dx)$ versus $\ell n(1-x)$ shown in Figure 12. For each energy, the cross section $d\sigma/dx$ is seen to drop rapidly as $(1-x)$ becomes smaller than m_p^2/s. Otherwise, all points lie approximately on the same straight line, in agreement with eq. (22).

AKNOWLEDGMENTS:

We are indebted to many people at the Fermi National Accelerator Laboratory who contributed to the success of this experiment, particularly the members of the Internal Target Laboratory. We acknowledge the support of the technical staff and our colleagues at Rockefeller University and the University of Rochester. We thank Dr. V. Rittenberg for many useful discussions. The Soviet members of the group express their deep gratitude to the State Committee for Utilization of Atomic Energy and to the Joint Institute for Nuclear Research (Dubna) for their generous support.

REFERENCES

1. M.L. Good and W.D. Walker, Phys. Rev. 120, 1857 (1960).
2. V.A. Nikitin et al, Preprint No. P1-7004, Dubna, USSR, 1973.
3. V. Bartenev et al, Phys. Rev. Letters 31, 1088 (1973). We use the same target as the hydrogen jet target used in this experiment. The characteristics of operating the jet with deuterium are very similar to those of hydrogen operation.
4. Baker et al. (To be published)
5. For the rise of the p-p total cross section between 200 and 400 GeV/c we have used the analytic formula $\sigma = 38.4 + 0.49\ \ln^2(s/122)$ given by Leader and Maor, Phys. Lett. 43B, 505 (1973).
6. We were guided by the results of G.G. Beznogikh et al, DUBNA Report No. E1-6615.
7. V. Bartenev et al. (To be published)
8. A.H. Mueller, Phys. Rev. D2, 2963 (1970).

FIGURE CAPTIONS

Figure 1 - Schematic drawing of the experimental arrangement.

Figure 2 - Mass of particles registered in a detector stack.

Figure 3 - Kinetic energy of recoil deuterons registered by a detector stack at fixed angle for various incident proton momenta.

Figure 4 - Elastic scattering differential cross section $d\sigma/dt$ for two different beam energies (a) 50 GeV/c and (b) 385 GeV/c. The curves have been normalized to the same arbitrary number at $t = 0$.

Figure 5 - The slope parameter $b(s)$ of elastic p-d scattering. Note that for p-p scattering, $s = 2m_p p_{LAB}$.

Figure 6 - Low mass region cross sections compared to proton-proton data.

Figure 7 - The missing mass spectrum for $0.03 < t < 0.04$ $(GeV/c)^2$.

Figure 8 - Differential cross section $d\sigma/dt$ for $m_x^2 = 10$ $(GeV/c^2)^2$.

Figure 9 - The slope parameter $b(m_x^2)$ of inelastic p-d scattering.

Figure 10 - The missing mass spectrum at $t = 0$.

Figure 11 - The integral of the inelastic cross section over t.

Figure 12 - The Feynman variable x distribution.

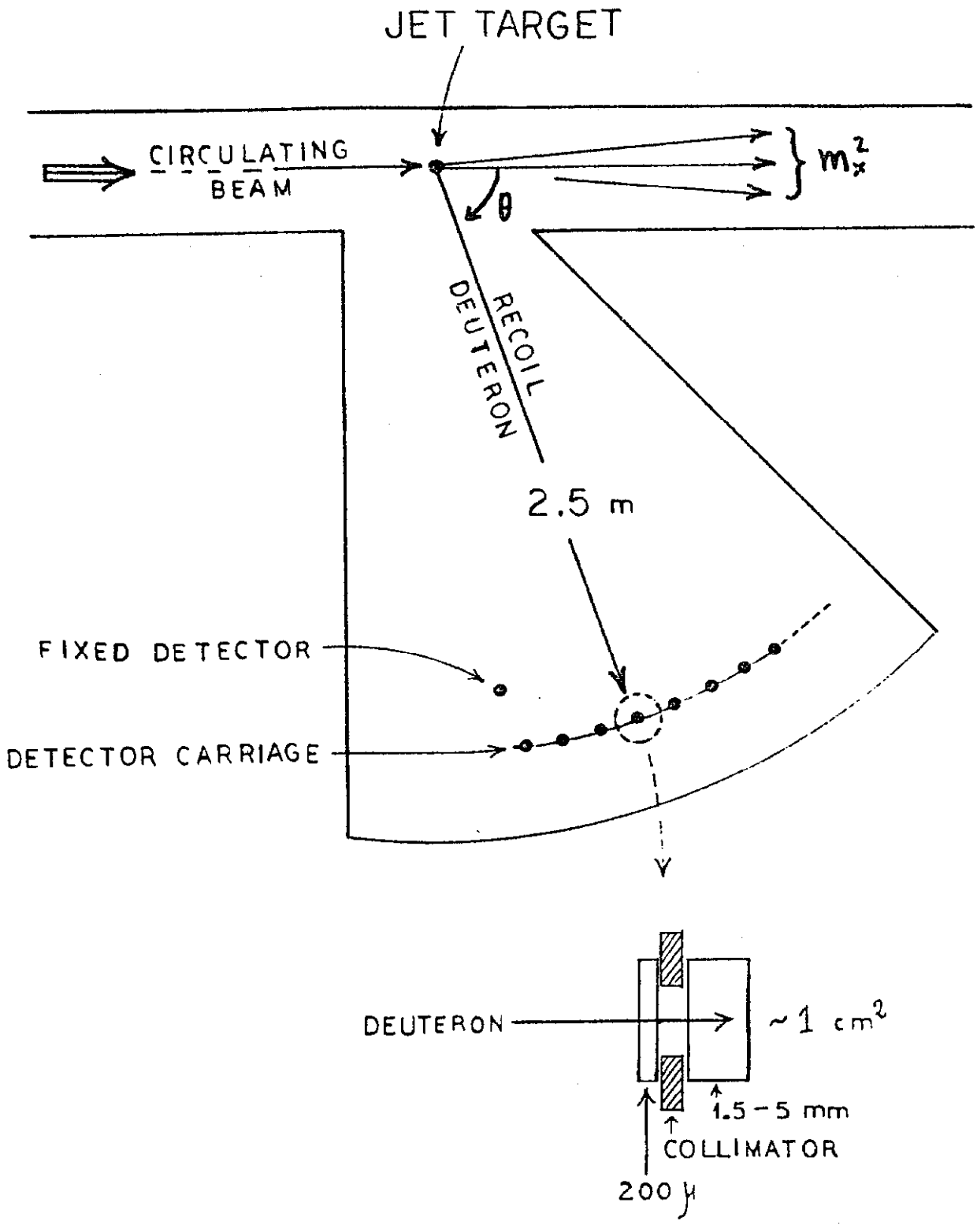
JET TARGET
CIRCULATING BEAM
m_x^2
θ
RECOIL DEUTERON
2.5 m
FIXED DETECTOR
DETECTOR CARRIAGE
DEUTERON
~1 cm²
1.5 – 5 mm
COLLIMATOR
200 μ

FIG. 1

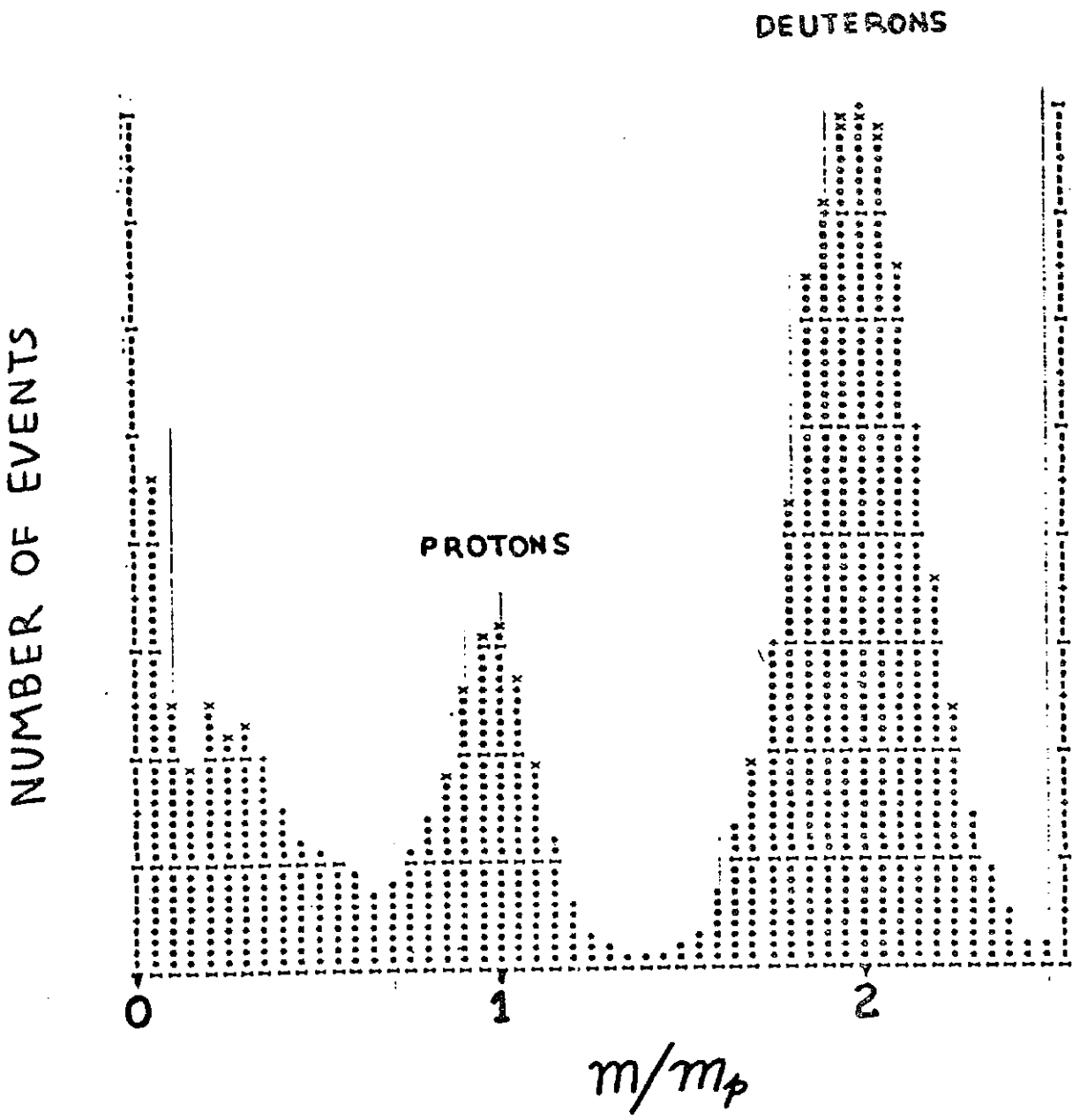

FIG. 2

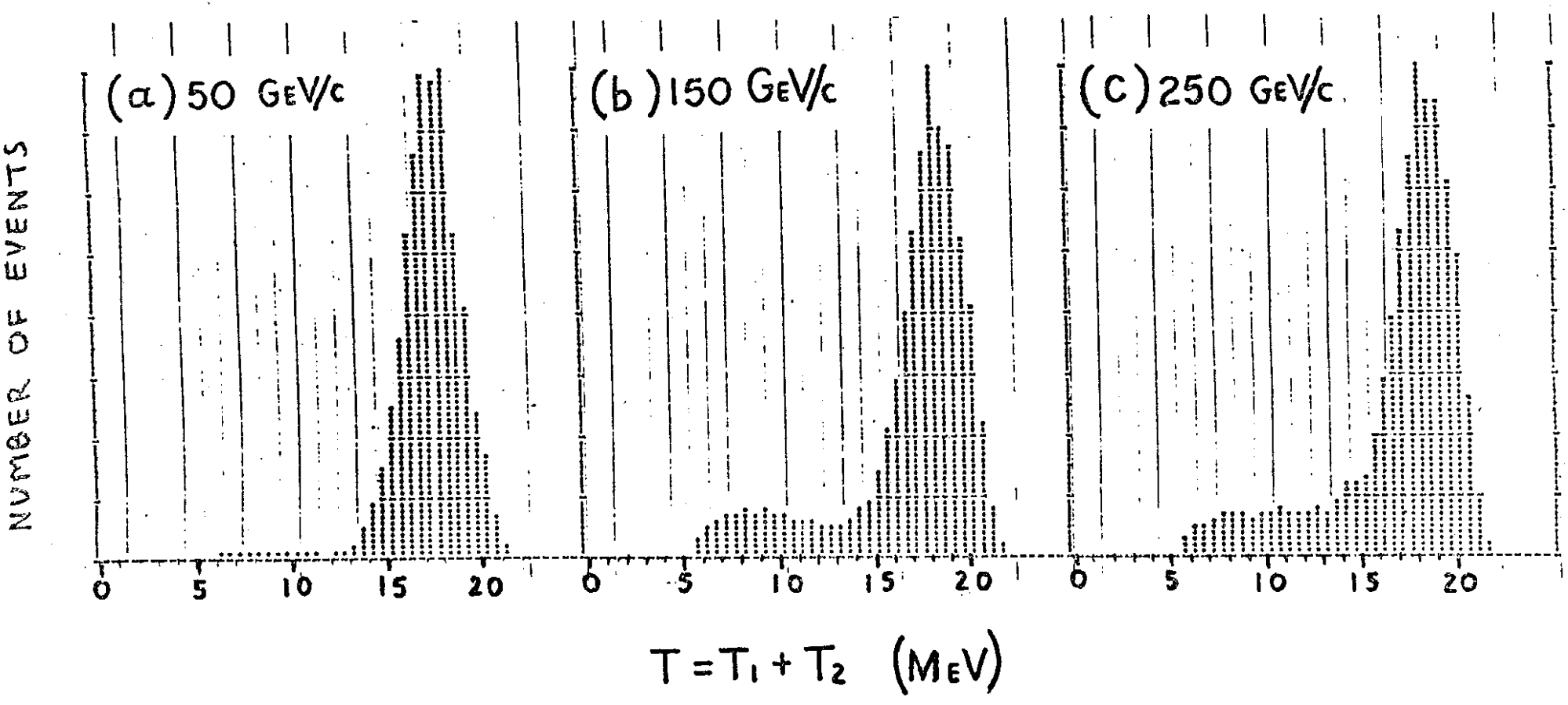
(a) 50 GeV/c
(b) 150 GeV/c
(c) 250 GeV/c
NUMBER OF EVENTS
0
5
10
15
20
T = T1 + T2 (MeV)

FIG. 3

Fig. 4

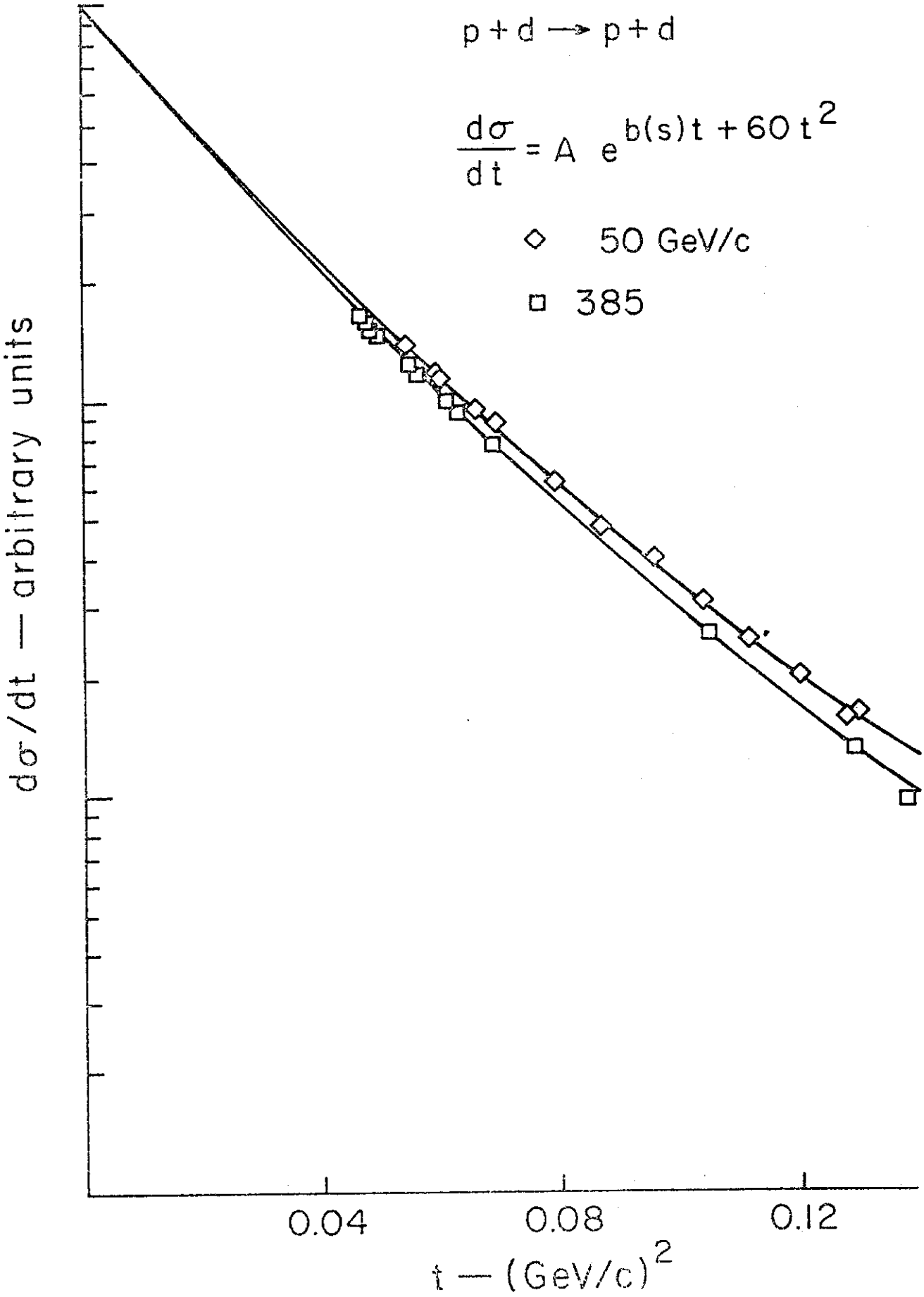
p + d → p + d
dσ/dt = A e^{b(s)t + 60 t^2}
◇ 50 GeV/c
□ 385
dσ/dt — arbitrary units
0.04
0.08
0.12
t — (GeV/c)^2

Fig. 5

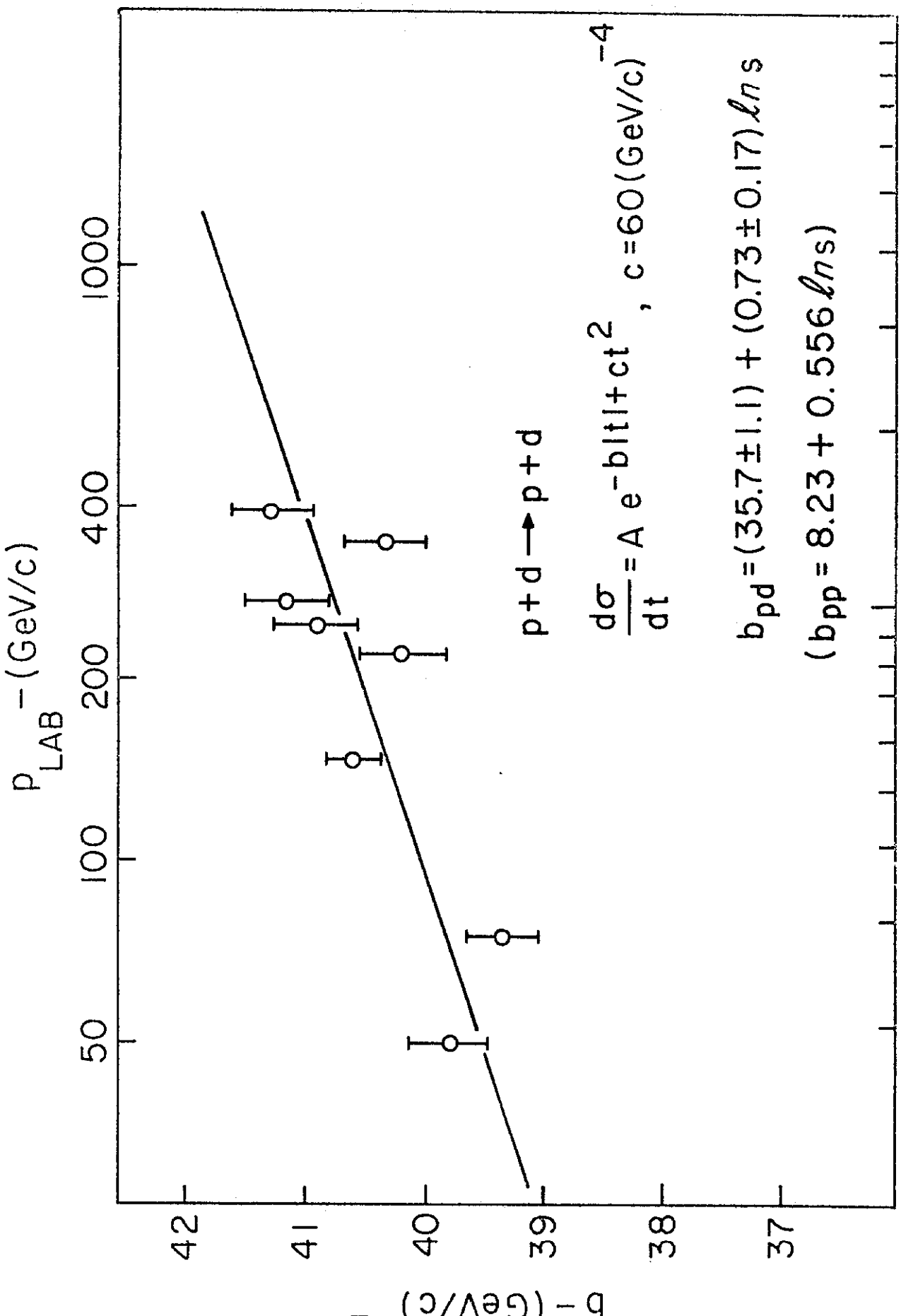
p_{LAB} − (GeV/c)
50
100
200
400
1000
1000
$S = 2 m_d p_{LAB}$ − GeV²
b − (GeV/c)⁻²
42
41
40
39
38
37
p+d → p+d
$\frac{d\sigma}{dt} = A\, e^{-b|t|+ct^2}$, c=60(GeV/c)⁻⁴
$b_{pd} = (35.7 \pm 1.1) + (0.73 \pm 0.17) \ell n\, s$
$(b_{pp} = 8.23 + 0.556\, \ell n s)$

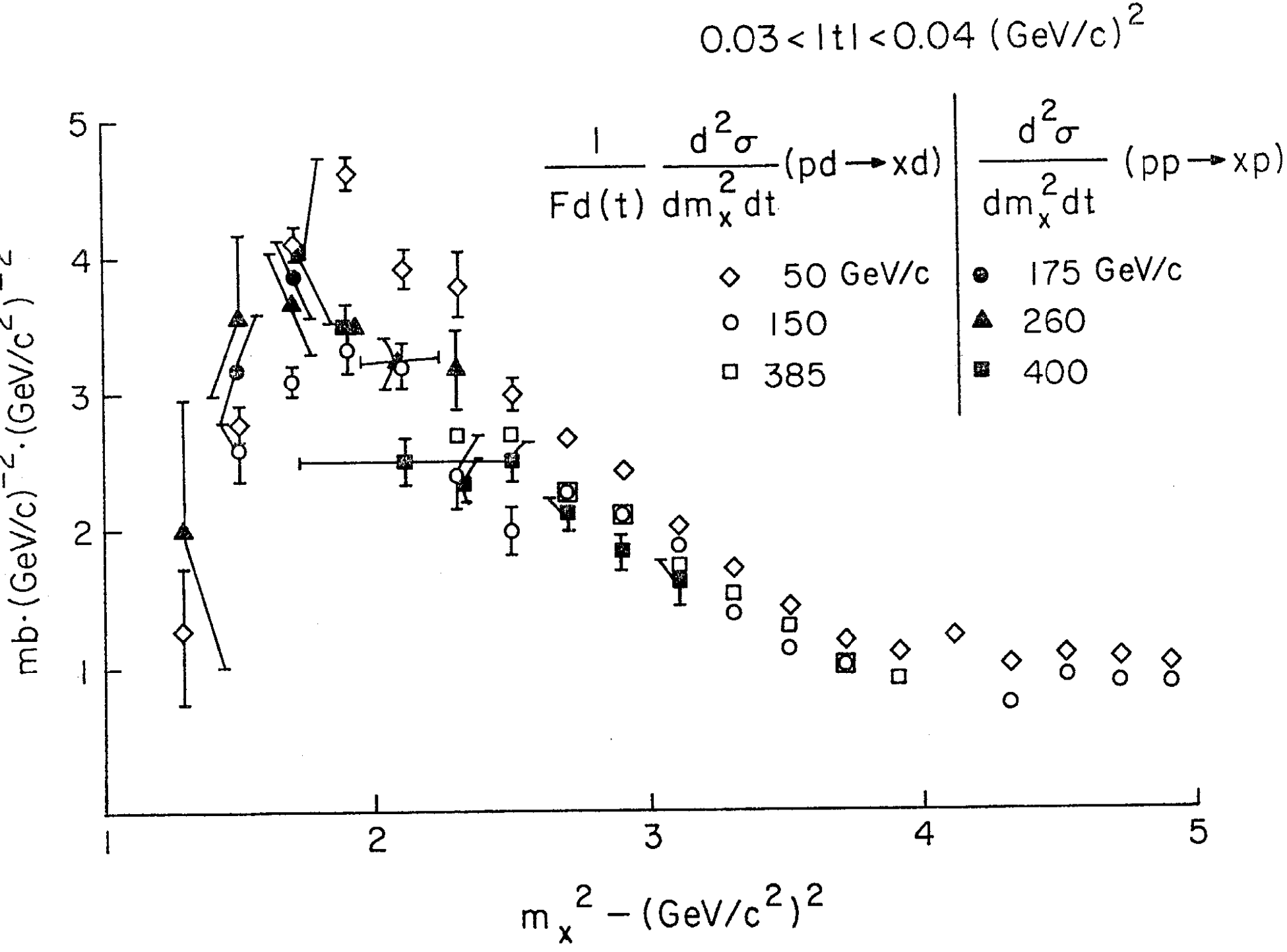
$0.03 < |t| < 0.04\ (GeV/c)^2$
$\frac{1}{Fd(t)} \frac{d^2\sigma}{dm_x^2 dt}(pd \to xd)$
$\frac{d^2\sigma}{dm_x^2 dt}(pp \to xp)$
50 GeV/c
150
385
175 GeV/c
260
400
$mb \cdot (GeV/c)^{-2} \cdot (GeV/c^2)^{-2}$
$m_x^2 - (GeV/c^2)^2$
1
2
3
4
5

Fig. 6

Fig. 7

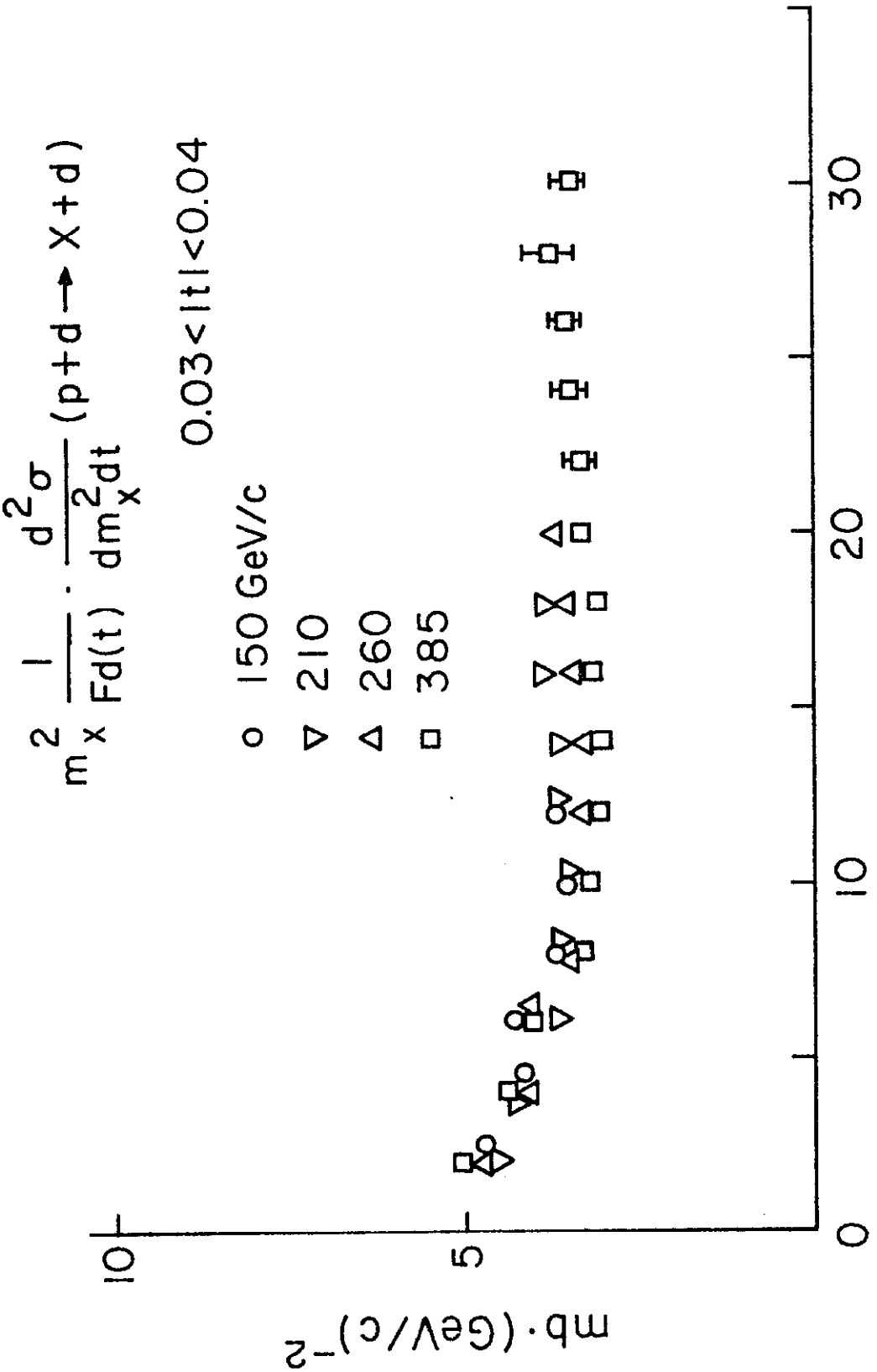
$\frac{1}{m_x^2 Fd(t)} \cdot \frac{d^2\sigma}{dm_x^2 dt}(p+d \rightarrow X+d)$
0.03<|t|<0.04
150 GeV/c
210
260
385
mb·(GeV/c)$^{-2}$
10
5
0
10
20
30
$m_x^2 - (GeV/c^2)^2$

Fig. 8

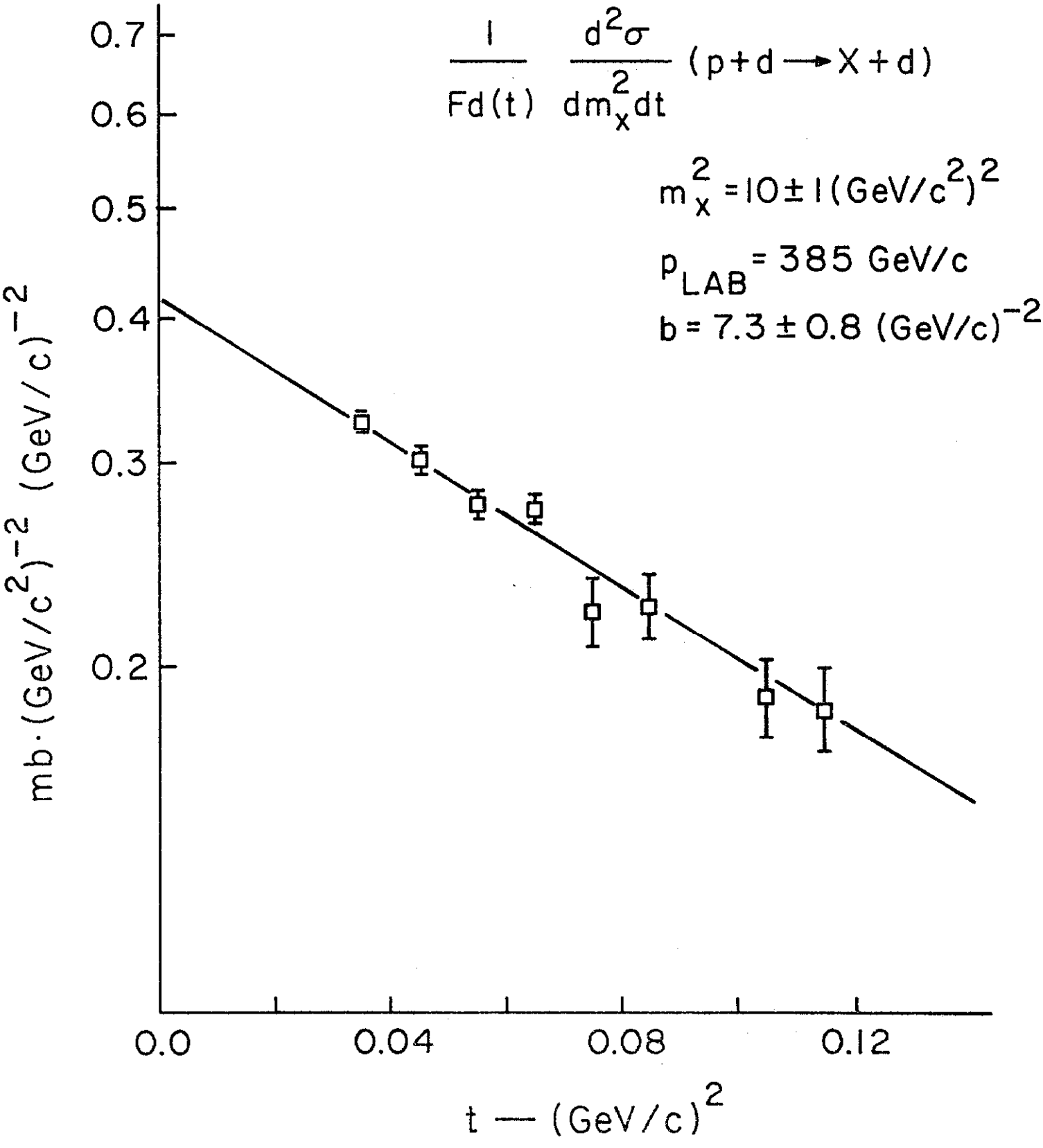
$\frac{1}{Fd(t)} \frac{d^2\sigma}{dm_x^2 dt} (p+d \rightarrow X+d)$
$m_x^2 = 10 \pm 1 (GeV/c^2)^2$
$p_{LAB} = 385$ GeV/c
$b = 7.3 \pm 0.8 (GeV/c)^{-2}$
$mb \cdot (GeV/c^2)^{-2} (GeV/c)^{-2}$
0.7
0.6
0.5
0.4
0.3
0.2
0.0
0.04
0.08
0.12
t — $(GeV/c)^2$

Fig.9

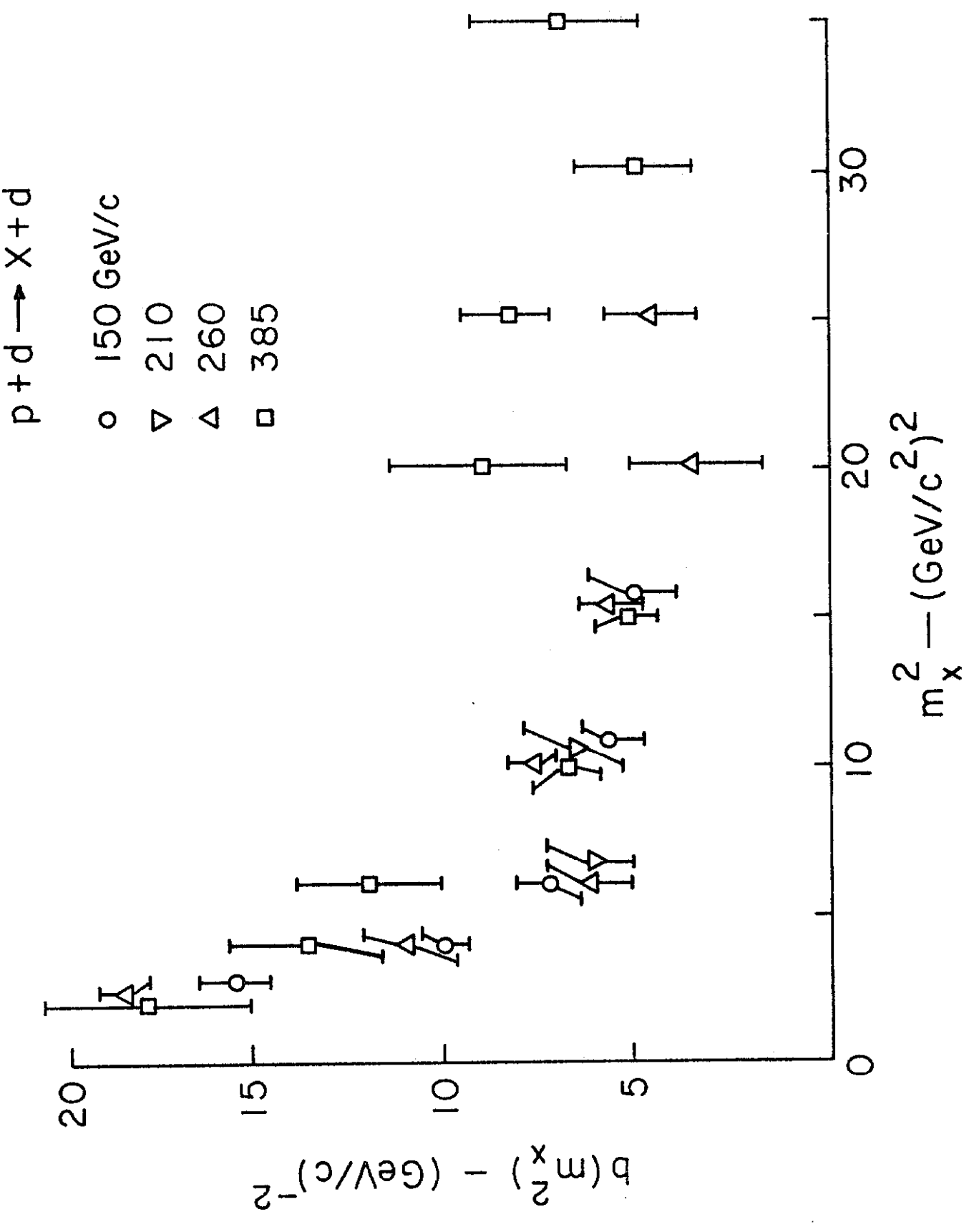
p+d → X+d
o 150 GeV/c
▽ 210
△ 260
□ 385
b(m²x) − (GeV/c)⁻²
20
15
10
5
0
10
20
30
m²x − (GeV/c²)²

Fig. 10

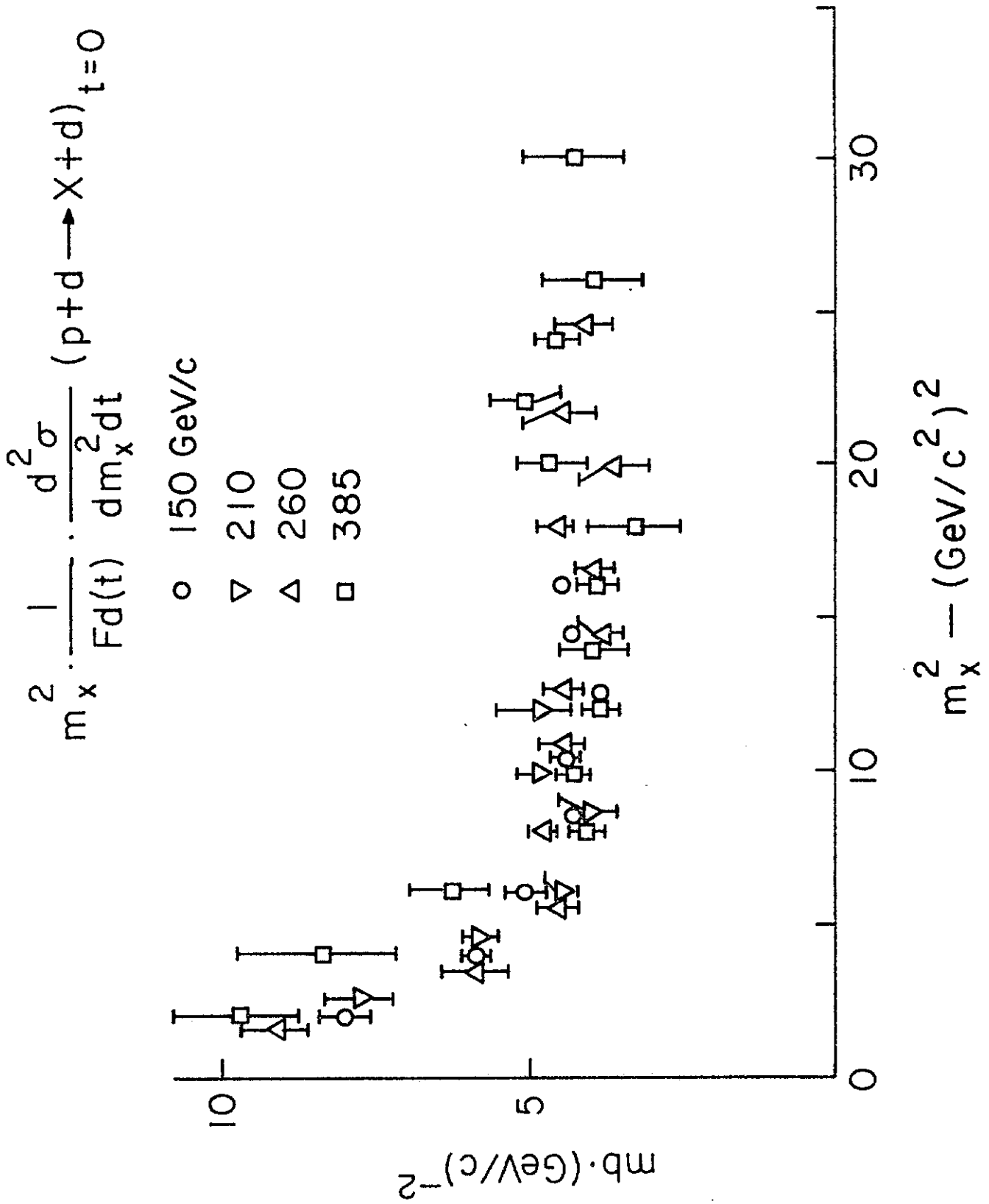
$m_x^2 \cdot \frac{1}{Fd(t)} \cdot \frac{d^2\sigma}{dm_x^2 dt} \quad (p+d \rightarrow X+d)_{t=0}$
o 150 GeV/c
▽ 210
△ 260
□ 385
mb·(GeV/c)$^{-2}$
10
5
0
10
20
30
m_x^2 — (GeV/c^2)^2

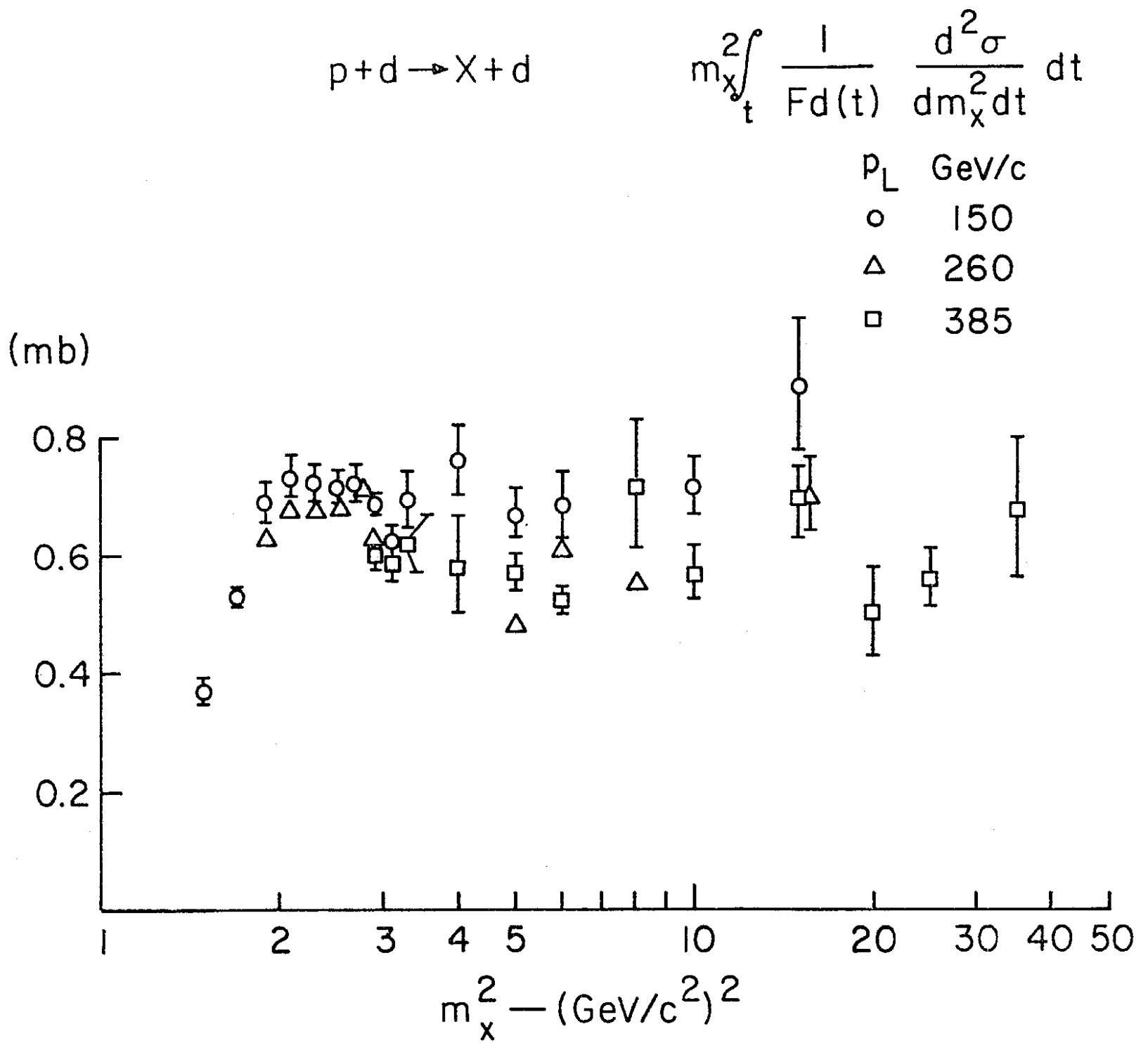
p+d → X+d
$m_x^2 \int_t \frac{1}{Fd(t)} \frac{d^2\sigma}{dm_x^2 dt} dt$
p_L GeV/c
○ 150
△ 260
□ 385
(mb)
0.8
0.6
0.4
0.2
1
2
3
4
5
10
20
30
40
50
$m_x^2 - (GeV/c^2)^2$

Fig. 11

Fig. 12

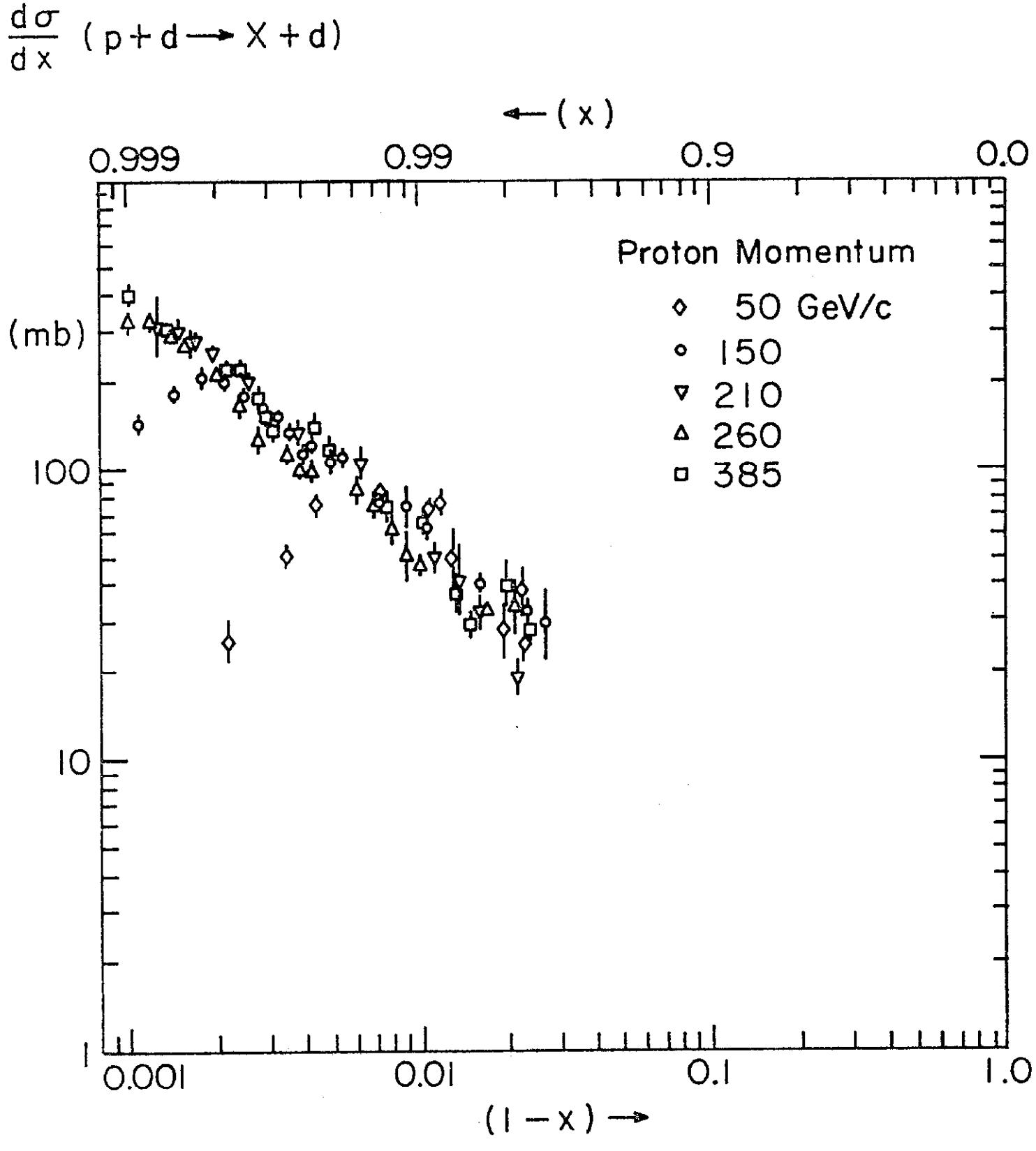
dσ/dx (p+d → X+d)
← (x)
0.999
0.99
0.9
0.0
Proton Momentum
50 GeV/c
150
210
260
385
(mb)
100
10
1
0.001
0.01
0.1
1.0
(1 − x) →